Soft Matter

PAPER

View Article Online
View Journal | View Issue

Cite this: *Soft Matter*, 2022, **18**, 3594

Transient response and domain formation in electrically deforming liquid crystal networks†

Guido L. A. Kusters, *[a] Paul van der Schoot [a] and Cornelis Storm[ab]

Recently, three distinct, well-separated transient regimes were discovered in the dynamics of the volume expansion of shape-shifting liquid crystal network films in response to the switching on of an alternating electric field [Van der Kooij *et al.*, *Nat. Commun.*, 2019, **10**, 1]. Employing a spatially resolved, time-dependent Landau theory that couples local volume generation to the degree of orientational order of mesogens that are part of a viscoelastic network, we are able to offer a physical explanation for the existence of three time scales. We find that the initial response is dominated by overcoming the impact of thermal noise, after which the top of the film expands, followed by a permeation of this response into the bulk region. An important signature of our predictions is a significant dependence of the three time scales on the film thickness, where we observe a clear thin-film-to-bulk transition. The point of transition coincides with the emergence of spatial inhomogeneities in the bulk of the film in the form of domains separated by regions of suppressed expansion. This ultimately gives rise to variations in the steady-state overall expansion of the film and may lead to uncontrolled patterning. According to our model, domain formation can be suppressed by (1) decreasing the thickness of the as-prepared film, (2) increasing the linear dimensions of the mesogens, or (3) their degree of orientational order when cross-linked into the network. Our findings provide a handle to achieve finer control over the actuation of smart liquid crystal network coatings.

Received 26th January 2022,
Accepted 21st April 2022

DOI: 10.1039/d2sm00125j

rsc.li/soft-matter-journal

1 Introduction

Liquid crystal networks comprise mesogens chemically cross-linked in a network, and resemble the perhaps more familiar liquid crystal elastomers.[1] Both materials respond mechanically to external stimuli such as a temperature variation,[2,3] UV irradiation,[4,5] or an electric field.[6–8] For the case of liquid crystal elastomers, in which the mesogens are incorporated in an elastomeric polymer network, this has already been exploited in the form of, *e.g.*, soft actuators,[9–15] shape-memory materials,[16–20] and haptic feedback.[21–25]

Although liquid crystal networks consist in essence of the same molecular building blocks as liquid crystal elastomers, the density of permanent crosslinks and mesogens is much larger. This turns out to produce a markedly different response characterised by not only macroscopic changes in shape but also in volume, the latter of up to ten percent, upon actuation.[6–8] Conventional liquid crystal elastomers, on the other hand, deform at approximately constant volume upon actuation. This suggests that liquid crystal networks enable potentially even richer applications in the field of smart coatings, *e.g.*, with controllable surface topographies,[3,6–8,26,27] adaptive adhesion and friction,[28,29] and control over the transport of molecular cargo.[2,30]

For such potential applications to come to fruition, the time scales on which they can be activated, *i.e.*, the transient response that must occur before a steady state is reached, must be addressed. This is especially relevant in light of the recent experimental work of Van der Kooij and co-workers,[7] who consider an electrically responsive liquid crystal network, comprising of two distinct species of mesogen (see Fig. 1): (i) mesogens that form permanent crosslinks in the polymer network (orange), and (ii) end-on grafted side-group mesogens, functionalised with a strong, permanent dipole moment (green). Due to their crosslinking into a network, the former are much less mobile than the latter, confirmed in previous work by results from molecular dynamics computer simulations.[31] The liquid crystal networks are synthesised on a substrate enforcing homeotropic alignment of the mesogens, and an alternating electric field (indicated in red in the figure) is subsequently applied in the direction perpendicular to the director field, so in the plane of the support of the film. Typical dimensions for the liquid crystal network film are 2.5 μm for the thickness and 0.5 × 0.5 mm for

[a] *Eindhoven University of Technology, Department of Applied Physics, 5612AZ Eindhoven, The Netherlands. E-mail: g.l.a.kusters@tue.nl*
[b] *Eindhoven University of Technology, Institute for Complex Molecular Systems, 5612AZ Eindhoven, The Netherlands*

† Electronic supplementary information (ESI) available: Full derivation of the theory in text format, and dynamics of order parameter profiles in video format. See DOI: https://doi.org/10.1039/d2sm00125j

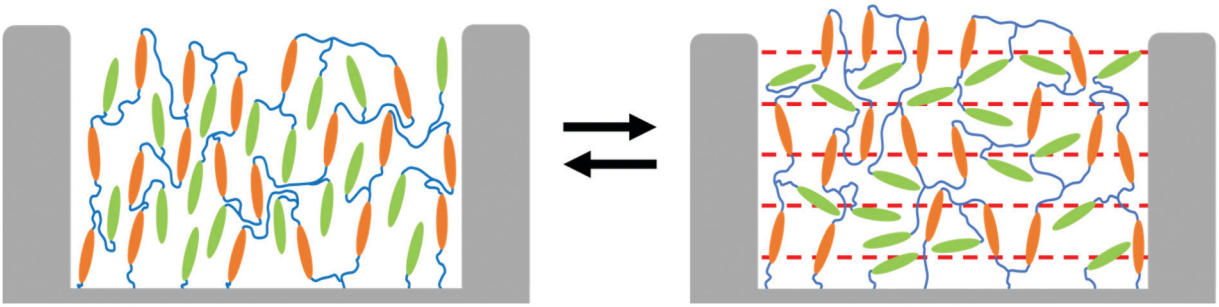

Fig. 1 Schematic representation of the liquid crystal network film, sandwiched between two grey electrodes, in the absence (left) and presence (right) of an electric field (dashed red lines). Cross-linked mesogens are indicated in orange, pendant (dipolar) mesogens are indicated in green and polymer strands are indicated in blue. The black arrows indicate the transition between the "off" state (left) and the "on" state (right) of the liquid crystal network. Figure adapted from prior work.[32]

the activated area, while the applied electric field strengths lie in the range of 1–10 V μm^{-1}.

Van der Kooij and co-workers report that, upon actuation, the liquid crystal network invariably undergoes three distinct, temporally well-separated regimes before the steady state response is reached in which significant volume increases of up to ten percent can be sustained.[7,8] Interestingly, the time scales on which these regimes occur are significantly larger than that of the actuation itself, with typical oscillation frequencies being in the range of hundreds of kilohertz. The material generally only enters its steady state after tens of seconds. A phenomenological explanation for the existence of a staged response before a steady state is reached is provided by van der Kooij *et al.* in terms of the fast response of the side-group mesogens, the delayed response of the cross-linked mesogens, followed by the sluggish, progressive weakening of the polymer matrix due to coherent oscillations of the mesogens.[7,8]

Whilst plausible, we here offer an alternative explanation, based on a spatially resolved, time-dependent Landau theory that couples local volume generation to the degree of orientational order of mesogens that are part of a viscoelastic network. According to our model, three time scales appear naturally from how in its response to the switching on of an AC field, the film first has to overcome the impact of thermal noise, subsequently reorients pendant mesogens starting at the top of the film and sets up a volume expansion, both of which then permeate through the film. This suggests that spatial information translates directly to distinct dynamical behaviour on an experimentally observable scale.

Our approach differs from that of Warner, Terentjev and co-workers, who pioneered a theoretical framework for liquid crystal elastomers combining the classical theory of rubber elasticity with the Landau-de-Gennes theory of liquid crystals, in which the polymer chains that are part of the network effectively perform anisotropic random walks, biased by the presence of liquid-crystalline mesogens.[33,34] This celebrated, "neo-classical" framework explains, among other things, the occurrence of mechanically induced nematic phase transitions and soft modes of deformation.[35–47] We require a different approach for two reasons. First, the polymer strands connecting the mesogens in the liquid crystal network are too short to effectively explore a random walk, implying the principles of the neo-classical theory no longer apply. Second, even if we were to apply this framework and adapt it to allow for non-volume-preserving deformations, then the predicted changes in volume are too small to explain the experimental observations.[48]

To address this problem, we proposed in previous work a dynamical Landau–de Gennes theory that focuses primarily on the state of the mesogens, rather than on the configuration of the network itself.[31,32] The motivation for this choice is that the liquid crystal network is dominated by the mesogenic component. The network properties enter on the one hand through the coupling of the nematic order to a local volume change, and on the other to a viscoelastic response that relaxes any volume changes. We obtained qualitative agreement between the theory for bulk systems and results of molecular dynamics computer simulations and experiments.[31] We have also characterised how in a thin-film geometry the volumetric response of the network to the switching on of a constant electric field permeates through the liquid crystal network from the top to the bottom.[32] In the current work, we apply our theoretical framework to investigate the response of thin-film liquid crystal networks to alternating electric fields, focusing specifically on the transient response. This allows us to probe the time scales on which the material can be activated.

The remainder of this paper is structured as follows. In Section 2, we provide a more detailed description of our model system, based on the experimental system studied by Liu, van der Kooij and co-workers,[6–8] and introduce the relevant theory, in Section 3. In Section 4, we illustrate the typical response of the liquid crystal network to an alternating electric field, focusing on the transient dynamical behaviour. Three characteristic time scales emerge naturally from the theory, as already advertised. The phenomenology of the processes associated with these time scales turns out to depend only weakly on the frequency of the alternating field, even though the steady-state volume change itself does depend strongly on the frequency. In Section 5, we study how these time scales vary with the thickness of the film, and recover a clear thin-film-to-bulk transition. This transition is characterised by the onset of the formation of expanded domains separated by regions of suppressed expansion, which arguably give rise to variations in

the steady-state overall expansion of the film and hence may lead to uncontrolled patterning. Next, in Section 6, we contextualise our results by quantifying the number of formed domains as a function of our model parameters, and identify how, in practice, domain formation can be suppressed. Finally, we summarise our most salient findings and critically compare our results to the experiments of Van der Kooij and co-workers,[7] in Section 7.

2 Model

We consider as our model system a liquid crystal network of densely connected mesogens. In recent experimental work, on which we base the model,[6–8] such a network was realised by synthesising acrylate monomers of the forms (i) =oligomer–mesogen–oligomer= and (ii) =oligomer–mesogen in approximately equal number. Since no additional polymer component is present, these monomers form the network themselves, rather than binding to it. This implies that the resulting network does not typically conform to either the classical main- or side-chain geometries (see Fig. 1), and that macroscopic phase separation of the polymeric and mesogenic components is not possible. We refer readers interested in the details of the sample preparation to the relevant texts.[6–8]

Given that the extent of the short polymer strands incorporated in the acrylate monomers, which act as spacers, is on the scale of the mesogen length, the liquid crystal network is more liquid crystal-like than network-like, with the distribution of mesogens largely determining the mechanical properties of the material. The crosslinking fraction, for example, follows directly from the ratio in which the acrylate monomers are used, since each free acrylate end can form two covalent bonds. We do not vary this quantity in this paper.

From the acrylate monomers we recognise the distinct species of cross-linked (orange) and pendant (green) mesogen discussed in the introduction, and shown in Fig. 1, which form the basis of our model. Although, due to its generic nature, the model encompasses various underlying mechanisms, ranging from an electrically-driven glass transition to the collective motion of an array of coupled oscillators,[32] here we focus on excluded-volume arguments. That is, upon application of the electric field, the pendant, dipole-functionalised mesogens reorient in response to it, whereas the cross-linked mesogens remain relatively immobile. This increases their mutually-excluded volume, and in turn the total volume of unoccupied space in the liquid crystal network. The collective effect of many such reorientations effects a macroscopic expansion of the material.[6–8]

In practice, steady-state operation of these liquid crystal networks requires alternating electric fields, as the polymeric material continually rearranges to fill the generated pockets of free volume. To emulate this balance in the model, we include a phenomenological, viscoelastic relaxation of the liquid crystal network volume. The resulting model is the same as that in our previous publication, albeit that we apply a slightly modified boundary condition.[32]

In the following section we briefly summarise the theory that we use for the analysis presented in the remainder of this paper. We refer readers interested in the details to the ESI.†

3 Theory

We describe the state of the liquid crystal network in terms of two order parameters: (1) the population fraction $0 \leq f^2 \leq 1$, representing the fraction of dipolar mesogens that align with the electric field, and (2) the volume-expansion order parameter $\eta = (V - V_0)/V_0$, which expresses changes in the system volume V relative to its initial value V_0. The relaxational dynamics of these non-conserved order parameters follows

$$\begin{aligned} \partial_t f &= -\Gamma_f \frac{\delta G}{\delta f} + \theta_f, \\ \partial_t \eta &= -\Gamma_\eta \frac{\delta G}{\delta \eta} + \theta_\eta - \gamma(\eta - \eta_0)\tau(z_0, t), \end{aligned} \tag{1}$$

where Γ_f and Γ_η denote standard kinetic coefficients, G is a free energy that is a functional of the two order parameters, and θ_f and θ_η are Gaussian noise terms obeying the fluctuation–dissipation theorem.[49] On the second line we added a term proportional to the phenomenological constant γ to effect the relaxation of η toward its initial profile η_0. We multiply this term by the relaxation function $\tau(z_0, t)$, as the viscoelastic relaxation of the network depends on the local deformation history. See the ESI† for the details.

For the free-energy functional we write

$$\begin{aligned} \frac{G}{A} = \int_0^{L_0} \mathrm{d}z_0 \Bigg[g_1 + g_2 + \frac{{\kappa_f}^2}{2(1+\eta(z_0))^2}\left(\frac{\partial f(z_0)}{\partial z_0}\right)^2 \\ + \frac{{\kappa_\eta}^2}{2(1+\eta(z_0))^2}\left(\frac{\partial \eta(z_0)}{\partial z_0}\right)^2 \Bigg], \end{aligned} \tag{2}$$

where the integral runs over the initial thickness of the film L_0, and A denotes the cross-sectional area. Hence, our model is quasi one-dimensional. The first term in eqn (2) is associated with the population fraction order parameter, according to

$$g_1 = \frac{1}{2}(H_* - H)f^2 + \frac{1}{4}B_f f^4. \tag{3}$$

This implies that the external field H drives mesogen reorientation if it exceeds a critical value H_*, with B_f a bulk-modulus-like coefficient. Experiments suggest that to overcome this critical field strength, in practice an electric field of approximately 4–5 V μm^{-1} is required in the frequency range of 600–900 Hz.[6] The second term in eqn (2) is associated with the volume-expansion order parameter, according to

$$g_2 = -\xi\eta f^2 + \frac{1}{2}B_\eta \eta^2. \tag{4}$$

This makes explicit the coupling between volume expansion and mesogen reorientation, where ξ is the coupling constant and B_η denotes a bulk-modulus-like coefficient. The last two terms in eqn (2) represent standard square-gradient contributions, with coefficients κ_f and κ_η, where we have made

explicit the geometric significance of the volume-expansion order parameter $\eta(z_0)$. Finally, eqn (1) and (2) are subject to the boundary conditions $f(0) = \eta(0) = 0, f'(L_0) = 0$ and $\eta(L_0) = \xi/B_\eta$. For a discussion, we refer to the ESI.†

This establishes the theory that we use in the remainder of this paper, which we numerically integrate by means of a Forward Time Centred Space finite difference scheme. To facilitate this, and reduce the number of adjustable parameters, we scale all parameters to be dimensionless. Details can be found in the ESI.† Henceforth, we shall only refer to these scaled parameters, although we use the same symbols where possible for notational simplicity. The same applies to the scaled order parameters, both of which now take values between zero and unity. Using the above procedure, we next discuss the transient dynamics that the model gives rise to.

4 Transient dynamics

We investigate the evolution of the order parameter profiles in response to an alternating electric field.‡ Although in previous work[32] we already established a clear top-to-bottom permeation phenomenon after switching on a constant electric field, alternating actuation renders the response frequency dependent. This makes the phenomenology more subtle, only yielding the known DC response in the low-frequency limit. That being said, our qualitative results turn out to not depend strongly on the driving frequency of the alternating electric field, hence we show only results for a single frequency, $\omega = 0.04$.

Fig. 2(a) shows the population order parameter profile, $f(z_0)^2$, which represents the local mesogen response (*e.g.*, collective reorientation) as a function of the height in the film, z_0, at typical stages during actuation. The mesogen response starts entirely flat (solid curve, time scale I) and subsequently saturates at the free boundary of the film, $z_0/L_0 = 1$ (dashed curve, time scale II), before finally permeating the material and entering a steady-state oscillation (dotted curve, time scale III). The spatial asymmetry in growth rate stems from our boundary conditions, which ensure that mesogen reorientation is hampered to a lesser extent at the free boundary of the film than at the solid substrate onto which the material is clamped.

The response of the volume-expansion order parameter profile, $\eta(z_0)$, shown in Fig. 2(b), follows the same trend, albeit with an initial profile that is already non-uniform (solid curve, time scale I). This reflects the diffuse interface we model. The other crucial difference is that volume expansion only responds indirectly to the electric field, by proxy of mesogen reorientation. This suggests that time scale I, prior to which we see no response, corresponds to a delay until a strong enough mesogen response has developed to effect volume expansion against thermal noise. Videos of both order parameter profiles are available as ESI.†

Although the permeation phenomenon at display here is expected given the structure and boundary conditions of the theory—we reported on this previously[32]—the natural emergence of three distinct time scales, which we clarify and explain further below, is nontrivial and connects our work more closely with experiments. Since the reported findings on transient dynamics concern measurements of surface dynamics,[7,8] we make this connection explicit by introducing coarse-grained quantities to represent both order parameters on the macroscopic scale. We define an integrated measure for the mesogen response, $I_m(t) = \int_0^{L_0} \mathrm{d}z_0 f^2(z_0, t)$, which could be probed experimentally by means of Raman scattering[53] or birefringence measurements,[54] as well as for the film thickness, $L(t) = \int_0^{L_0} \mathrm{d}z_0 \left[1 + \frac{\xi}{B_\eta}\eta(z_0, t)\right]$. Here, we assume that the effect of any local reorientation or deformation instantaneously registers on the macroscopic scale, meaning such information propagates through the network on time scales much shorter than those under consideration. This we expect for the thin films used in the cited experiments, and implies that mesogen reorientation and volume expansion can macroscopically result in distinct changes in surface dynamics. Below we discuss the transient dynamics of both in order to pin down the relevant time scales (I, II, and III). For the numerical procedure we use, see note.§

Fig. 3 shows the temporal evolution of the integrated mesogen response, I_m, on a logarithmic scale. The inset shows the same curve on a linear scale. The curve is segmented by vertical red lines, which coincide with the order parameter profiles representing the time scales I, II, and III shown in Fig. 2. The solid red line (time scale I) has no special meaning in this figure, which shows that mesogen reorientation grows exponentially until the dashed red line (time scale II) is reached. At this point, the response saturates at the free boundary of the film. The linear-scale inset shows that the integrated mesogen response at this time is significantly lower than in the eventual steady state, indicating that the bulk response must also eventually play an important role. This is illustrated by the progress from the dashed to the dotted (time scale III) red line.

The concomitant expansion of the film, as shown in Fig. 4, follows the same pattern as described above, with one notable exception: prior to the solid red line (time scale I), the behaviour is

‡ The form $H \propto |\underline{E}|^2$ is appropriate for describing the free energy of an induced dipole due to the inversion symmetry of the nematic director $\underline{n} \to -\underline{n}$. Although for a mesogen with permanent dipole moment $\underline{p}$ the analogous expression would read $-\underline{p}\cdot\underline{E}$, averaging this over an ensemble of mesogens using a Boltzmann distribution this can again be written in the form $-\langle\underline{p}\cdot\underline{E}\rangle \propto |\underline{p}|^2|\underline{E}|^2$ for sufficiently weak electric fields, $|\underline{p}||\underline{E}| \ll k_\mathrm{B}T$.[50–52] Although this relationship becomes linear in the limit of strong electric fields, this does not alter our qualitative conclusions in this paper.

§ Numerically, we measure the time scales as follows. Since we expect the volume-expansion order parameter, η, to be characterised by thermal noise prior to time scale I, we determine the first time scale by keeping track of the relative expansion. The time scale then coincides with the last instance of successive time steps differing by more than 5%. Similarly, time scale II corresponds to a saturated mesogen response at the top of the film and, accordingly, we determine it by identifying the point in time where $f(L_0)$ first exceeds 95% of its maximum value. Finally, time scale III demarcates the onset of the steady-state oscillation, which we identify by computing the maximum relative expansion the liquid crystal network assumes in the steady state, and finding the first instance where the relative expansion lies between 99% and 101% of this value.

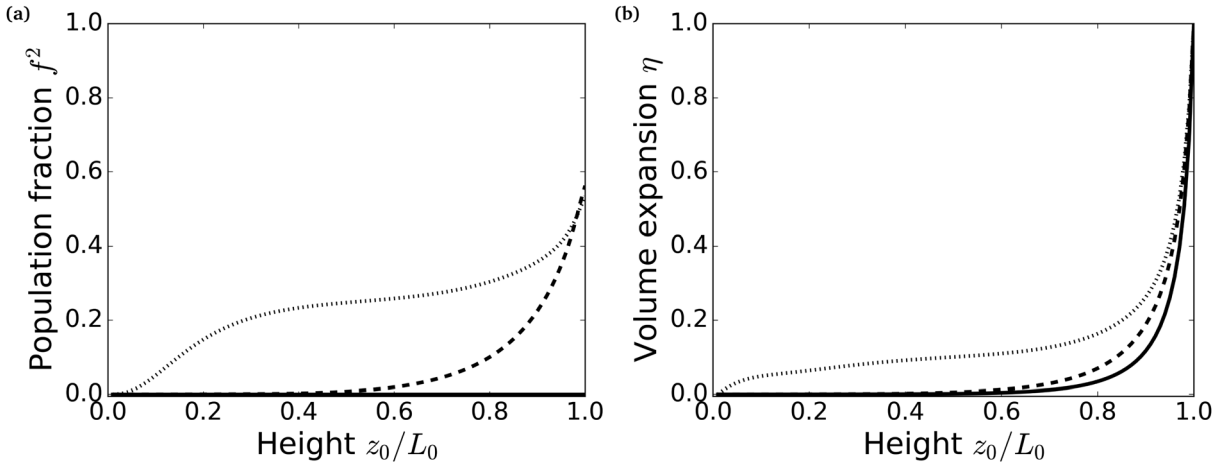

Fig. 2 Fraction of mesogens that respond to an applied electric field (a) and the volume increase of the liquid crystal network (b), obtained from the scaled theory and as a function of the scaled height coordinate z_0/L_0. We apply a super-critical alternating electric field, $(h+1)\cos^2 2\pi\omega t$, with scaled field strength and scaled driving frequency $\omega = 0.04$. The curves correspond to $t = 51.4$, $t = 100.5$, and $t = 140.1$. See the ESI† for the scaling procedure. The values used for the scaled model parameters are $\zeta = 0.51$, $B_f = 3.70$, $\eta(L_0) = 3.375$, $\kappa_f = \kappa_\eta = 0.071$, $\Gamma_f = 0.46$, $\Gamma_\eta = 1$, $\gamma = 0.285$, $\langle\theta_f^2\rangle = 3.78 \times 10^{-17}$, and $\langle\theta_\eta^2\rangle = 8.22 \times 10^{-17}$.

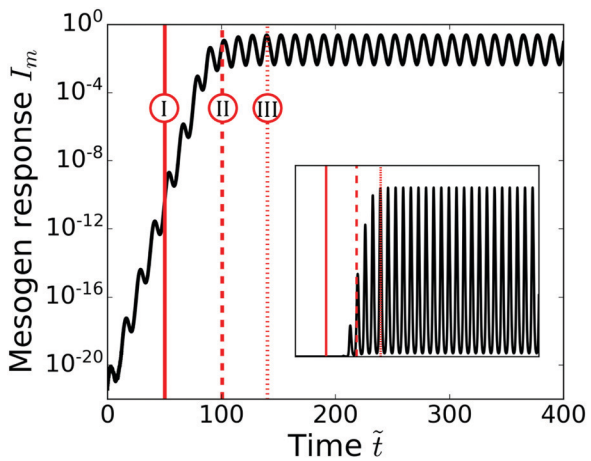

Fig. 3 Overall, integrated mesogen response, $I_m(t) = \int_0^{L_0} \mathrm{d}z_0 f^2(z_0, t)$, as a function of the scaled time t, shown on a semi-logarithmic scale. The vertical red lines correspond to the time scales I, II, and III, identified in Fig. 2 and discussed in Section 4, and the inset shows the same figure on a linear scale. See the ESI† for the scaling procedure and see Fig. 2 for the parameter values.

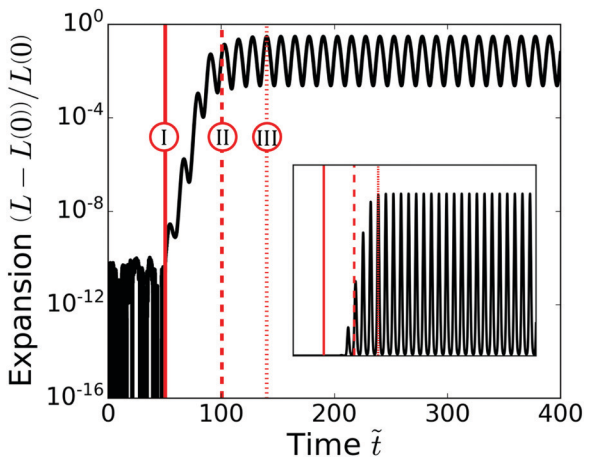

Fig. 4 Expansion of the liquid crystal network film, $(L(t) - L(0))/L(0)$, with $L(t) = \int_0^{L_0} \mathrm{d}z_0[1 + \eta(z_0, t)]$ the film thickness, as a function of the scaled time t, shown on a semi-logarithmic scale. The vertical red lines correspond to the time scales I, II, and III, identified in Fig. 2 and discussed in Section 4, and the inset shows the same figure on a linear scale. See the ESI† for the scaling procedure and see Fig. 2 for the parameter values.

entirely dominated by noise. As noted above, this is due to the fact that volume expansion is driven by mesogen reorientation, rather than directly through the applied electric field. We stress, however, that the expansion associated with this regime is so small in magnitude so as to fall outside the range of validity of our coarse-grained theory, which applies on length scales exceeding the mesh size of the network, *i.e.*, the distance between permanent crosslinks, $l \approx 10$ nm. This length scale we base on the size of the acrylate monomers used in the experimental efforts of Liu, Van der Kooij, and co-workers,[6–8] and it shall later return as a system parameter to enable predictions in terms of physical quantities. Below this length scale, the theory provides no meaningful insight, and so we are forced to disregard the corresponding dynamics: instead of directly observing the thermal noise, we recover no discernible response whatsoever. In practice, the time scale at which expansions on the scale of the network mesh size arise lies slightly beyond the solid red line. A similar limit of resolution exists in the experiments due to the limitations of the measurement set-up. After this, the dashed red line (time scale II) again corresponds to a saturated expansion at the top of the film and the steady state is reached at the dotted red line (time scale III).

Thus, assuming that the features discussed above translate to changes in surface dynamics, we recognise three characteristic

time scales, which split up the transient dynamics of the material into three distinct regimes, and for which our theory provides an explanation. First, prior to time scale I, a collective response of the mesogens builds up. During this regime, no appreciable volume changes are discernible. Secondly, between time scales I and II, we observe a local expansion of the liquid crystal network, focused at the top of the film. This is driven by local mesogen reorientation, which is impeded to a lesser extent at the free boundary of the film. Finally, between time scales II and III, the response permeates into the bulk of the material, and realises a steady-state oscillation. This ends the transient stages of dynamics: beyond this point the steady-state oscillation is sustained.

Our findings suggest that permeation of the response into the liquid crystal network film provides an alternative explanation for the three transient regimes Van der Kooij and co-workers report in their experimental work.[7] Our interpretation implies that spatial information translates directly to distinct dynamical behaviour on experimentally accessible scales, whereas the interpretation proposed by Van der Kooij and co-workers associates the regimes with the collective response of different mesogen species. To provide a test that distinguishes between the two, we devote the following section to investigating the effect of varying the (initial) film thickness.

5 Dependence on film thickness

We can probe the effect of the initial film thickness by varying the square-gradient coefficients, κ_f and κ_η. These coefficients describe the range of local interactions and, in particular, we have scaled them to be measured relative to the initial film thickness. Since the mesh size of the network, l, is the only microscopic length scale of the problem, we estimate $\kappa_f = \kappa_\eta \approx l/L_0$ and vary the initial film thickness, L_0, by proxy of κ_f and κ_η. Fig. 5 shows the resulting transient time scales, averaged over ten numerical simulations with random thermal noise, δ-correlated in both time and space.

In the figure, the black circles represent the time required to overcome the thermal noise (regime I), the blue triangles describe the the time it takes to obtain a saturated response at the top of the film (regime II), and the red squares give the time after which the material enters its steady-state oscillation (regime III). Reading the figure from left to right, it becomes apparent that a thin-film-to-bulk transition occurs, approximately, at $L_0 = 1$ μm if we presume $l \approx 10$ nm. Across this transition, the times required to overcome thermal noise and achieve a saturated response at the top of the film decrease sharply, whereas the time required to achieve a steady-state oscillation increases. We rationalise the former two by noting that decreasing the square-gradient coefficients weakens the local interactions within the model. If we make the film thicker, the range of mesogen-mesogen interactions shrinks relative to the thickness of the film. As a result, the inhibiting effect of the substrate onto which the film is clamped effectively affects an increasingly small proportion of the film. Consequently, a greater proportion of mesogens can reorient freely in response

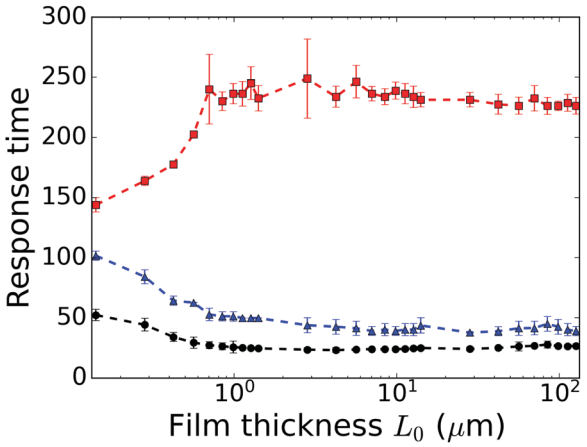

Fig. 5 Time scales I (black circles), II (blue triangles), and III (red squares) corresponding to the different transient regimes shown in Fig. 2 and discussed in Section 4, as a function of the (initial) film thickness, L_0, using a network cross-linking distance $l \approx 10$ nm (see Section 5). Data points and error bars are taken over ten numerical simulations with random thermal noise, and dashed lines are guides to the eye. See the ESI† for the scaling procedure and see Fig. 2 for the parameter values not explicitly stated here.

to an applied electric field, and the response accelerates. We attribute the fact that the steady-state oscillation nevertheless takes longer to establish to the onset of domain formation, which we demonstrate in the following section. Until then, we treat this as a working hypothesis.

If we compare our predictions with the work of Van der Kooij and co-workers,[7] we thus correctly identify three distinct transient time scales, and provide an explanation. Looking beyond this, we find that the magnitude of these transient time scales differ from the time scale of actuation by at most an order of magnitude, regardless of film thickness. Although this is more modest than the multiple orders of magnitude reported by Van der Kooij and co-workers,[7] it is not too surprising given the relatively simple and phenomenological nature of the theory. We shall return to this point in the discussion, in Section 7.

Finally, not shown in the figure, we find an additional transition for exceedingly large film thicknesses on the centimetre scale. These are not relevant length scales for the smart coatings we consider here, and so fall outside the scope of this paper.

The experimental implications of varying the film thickness are broader, however, than just altering the transient time scales of the liquid crystal network film. Fig. 6 illustrates that the steady-state volume expansion of the film is also affected. In particular, we find that in the thin-film limit (left), increasing the film thickness increases the magnitude of expansion, which approaches a constant value in the bulk limit (right). Furthermore, operation of the material becomes less predictable near the thin-film-to-bulk transition, around $L_0 = 1$ μm, as evidenced by the large error bars. This implies that a large spread of steady-state expansion can be expected when operating the liquid crystal network near the thin-film-to-bulk transition in

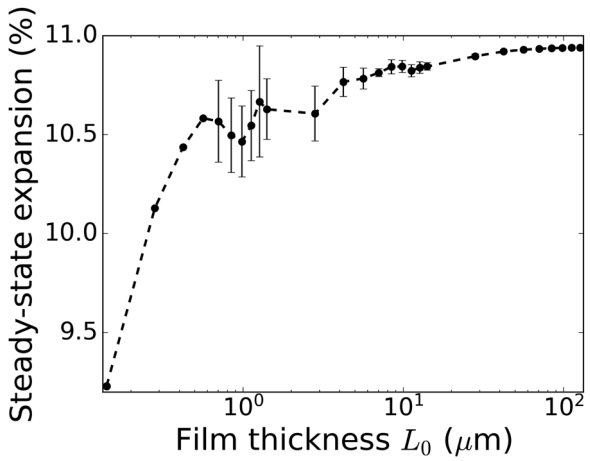

Fig. 6 Steady-state expansion of the liquid crystal network film, as a function of the (initial) film thickness, L_0. Data points, including error bars, correspond to an average over ten numerical simulations with random thermal noise, and dashed lines are guides to the eye. See the ESI† for the scaling procedure, and see Fig. 2 and 5 for the parameter values not explicitly stated here.

experiments. Although the figure shows a peak in the magnitude of the variance, in the following section we shall argue that the decrease of it entering the bulk regime stems from the limited spatial resolution of the model calculations. Indeed, we expect the increased variance to persist into the bulk regime, although this does not alter our other results. Thus, practically, there is a trade-off to be made, where swift, controlled steady-state actuation can be achieved in thin films at the expense of the overall deformation magnitude, whereas thick films achieve a greater deformation at the expense of more drawn-out transient dynamics and reduced control of the patterning.

This concludes our discussion of the effect the initial film thickness has on the transient dynamics. We point out that a similar dependence on initial film thickness is not expected if we assume the different transient regimes result from the collective reorientation of different mesogen species, as Van der Kooij and co-workers propose.[7] Accordingly, experiments on films with varying thicknesses could be used to further probe the underlying mechanism. Finally, as announced above, we demonstrate that the thin-film-to-bulk transition is indeed characterised by the onset of domain formation, which contextualises our results.

6 Domain formation

Fig. 7 shows the steady-state order parameter profiles for various values of the (initial) film thickness, L_0, offset by multiples of 0.3 for clarity. From this it is apparent that around $L_0 = 1$ μm (black curve) the system first splits into two domains, both characterised by a significant degree of mesogen reorientation and volume expansion. These domains are separated by a domain wall: a small region in which, locally, this response is significantly smaller than around it. The small bump that is visible at the centre of the domain wall in Fig. 7(b) stems from the fact that here the gradient in mesogen reorientation is largest. Such energetically unfavourable gradients can be smeared out by locally expanding the material. Consequently, regions in which the fraction of field-aligned mesogens varies significantly generally require more space than regions where this fraction varies weakly. Thus, the bump is a direct consequence of the geometric significance of the volume-expansion order parameter η.

Upon increasing the (initial) film thickness, L_0, the number of domains increases, as shown by the grey ($L_0 = 2$ μm) and light grey curves ($L_0 = 5$ μm). Simultaneously, the domain walls separating the different domains become narrower relative to the thickness of the film. Note that the positions of these domain walls are arbitrary, as the total free energy is invariant under their translation. This suggests repeated numerical simulations should yield domain walls at different positions, which indeed they do. In addition, it implies domain wall

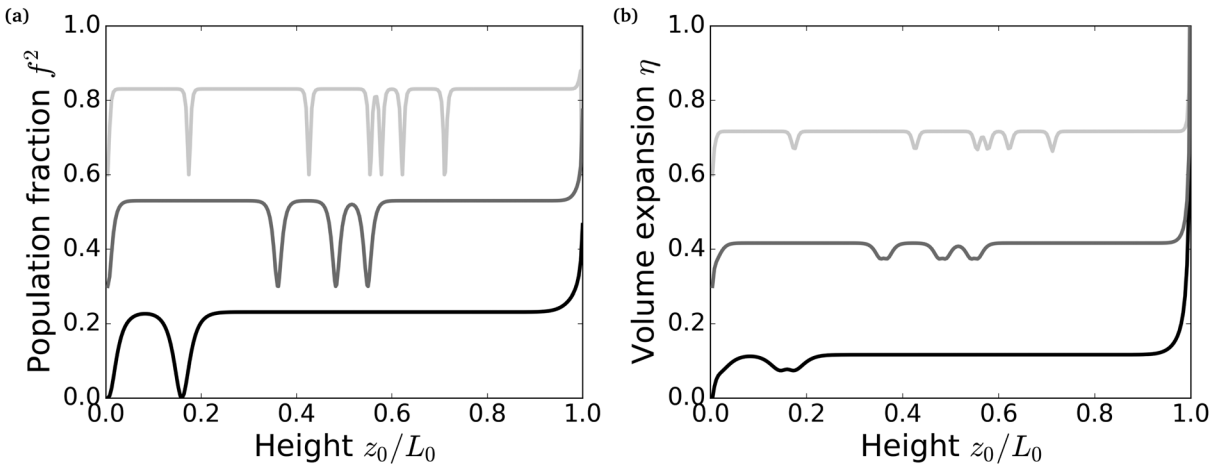

Fig. 7 Volume-expansion order parameter, η, as a function of the scaled height coordinate z_0/L_0. The different curves are offset by multiples of 0.3 for visual clarity, and correspond to the different (initial) film thicknesses $L_0 = 1$ μm (black), $L_0 = 2$ μm (grey), and $L_0 = 5$ μm (light grey). See the ESI† for the scaling procedure, and see Fig. 2 and 5 for the parameter values not explicitly stated here.

motion as a function of time, although this process becomes exceedingly slow for the small ratio of noise to the characteristic energy scale of the problem, the critical field strength, H_*, we use, combined with the limited spatial resolution of our numerical implementation.

Mathematically, we can interpret the different domains by more closely inspecting the population order parameter. Although only f^2 couples to volume expansion, and is the physical quantity of interest representing the fraction of coherently reorienting mesogens, in our dynamical equations (eqn (1)) we explicitly compute the value of f to recover this quantity. This means that while the model is explicitly constructed as a function of f^2, solving the dynamical equations also grants access to the auxiliary field f. As it turns out, neighbouring domains exhibit the same magnitude but opposite signs for f, as shown by Fig. 8. Thus, one way of interpreting our findings is by associating different signs of f with different modes of mesogen reorientation. Since within the model assumptions parallel and anti-parallel alignment of the dipolar mesogens with the electric field carry the same free energy, a possible candidate for this would be coherent mesogen reorientation in phase and in anti-phase with the field. This would imply that in neighbouring domains the mesogens oscillate coherently in opposite directions, with the oscillation being smothered in the domain wall between them, due to their mutual (excluded-volume) interactions.

The fact that domain formation occurs at all suggests that permeation of the response is sufficiently slow so as not to permeate the material before the bulk response ensues. Accordingly, the bulk response is not absorbed by a permeating front and it takes longer for the steady-state oscillation to be established (see Fig. 5), since the bulk response must then grow virtually unaided by permeation.

Likewise, we attribute the variable steady-state expansion of the liquid crystal network beyond the thin-film-to-bulk transition (see Fig. 6) to the onset of domain formation. For thin films, the formation of domains is suppressed by the inhibiting effect of the substrate onto which the material is clamped. This results in a finely controlled response. However, as we increase the film thickness beyond the system's correlation length, this inhibiting effect does not penetrate as deeply into the bulk anymore, and entropy dictates that the number of formed domains, as well as their variance, grows accordingly. This explains the sharply increased variance of the steady-state expansion since each domain wall represents a region of suppressed expansion.

Considering that the correlation length must be independent of system size for thick films, and that the spread in the number of domains scales with the system size, we conclude that the variance in the expansion of the film must remain large in the bulk regime. As announced, in Fig. 6, we instead obtain a reduced variance upon approaching the bulk limit due to limited spatial resolution of our calculations. In other words, while we can accurately determine the number of formed domains given our numerical discretisation, we lack the resolution to accurately measure the suppressed expansion induced by the corresponding domain walls that become negligibly narrow in the bulk limit. We reiterate that this does not influence our remaining results, which we have scaled with this limitation in mind.

Finally, we quantify our claims regarding domain formation by computing the average number of domains as a function of the initial thickness of the film. This number of domains, normalised by the number of lattice sites used in our numerical scheme, is shown in Fig. 9. The black data points show that the onset of domain formation indeed occurs around $L_0 = 1$ μm, beyond which it steadily grows until it saturates around $L_0 = 100$ μm. This is also roughly the point at which both the time scales corresponding to the different transient regimes, as well as the magnitude of steady-state volume expansion, plateau.

We can straightforwardly understand the asymptotic value the domain fraction, d, assumes by considering that in the bulk limit (right) local interactions are negligible. Consequently, the problem of determining the number of expected domains is equivalent to determining the number of clusters in an array of ideal, non-interacting spins in one dimension. For a large array size $N \gg 1$, edge effects become negligible and each subsequent spin has an equal probability of introducing an additional domain or not. This suggests the domain fraction must approach $d = 1/2$ in the bulk limit, as indicated by the dotted red line.

Furthermore, although the approach toward this asymptotic value is significantly more complicated in terms of both energetic and entropic considerations, we provide a rough estimate on the qualitative behaviour. This we do by investigating the linear stability of infinitesimal perturbations of the form $\sin\frac{2n-1}{2}\pi z_0$ in our theory, where $n = 1, 2, 3, \ldots$ represents the number of domains. These perturbations obey the boundary conditions by construction. For the purpose of this calculation, we consider only the population order parameter, f^2, as it

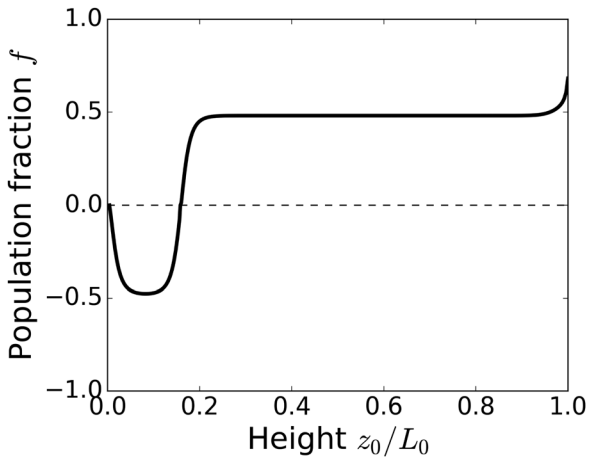

Fig. 8 Population order parameter profile, f, as a function of the scaled height coordinate z_0/L_0. We can interpret the sign of f as indicative of different modes of mesogen reorientation. See the ESI† for the scaling procedure, and see Fig. 2 and 5 for the parameter values not explicitly stated here.

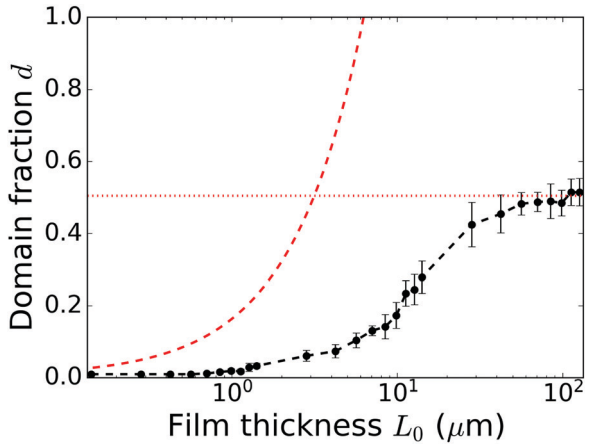

Fig. 9 Number of domains per lattice site used in our numerical scheme, d, as a function of the (initial) film thickness, L_0. Black data points, including error bars, correspond to an average over ten numerical simulations with random thermal noise, and the dashed black lines are guides to the eye. The dashed red curve indicates the limit of stability following a simple linear stability analysis (see eqn (5)), and the dotted red line denotes the asymptotic limit d = 1/2. See the ESI† for the scaling procedure, and see Fig. 2 and 5 for the parameter values not explicitly stated here.

dominates the (linear) model dynamics.[32] We solve the resulting dispersion relation to identify which modes become unstable and which damp out, yielding

$$n = \frac{1}{\pi\kappa_f}\sqrt{\frac{H}{2H_*}} + \frac{1}{2}, \tag{5}$$

as the limit of stability. Here, we made our results independent of the driving frequency, ω, by assuming the alternating electric field oscillates sufficiently quickly for the liquid crystal network to effectively 'feel' only the average field. Although this estimate, shown by the dashed red line in Fig. 9, clearly overestimates the expected domain fraction, neglecting the explicit growth rates, non-harmonic modes, lower-order modes, and the number of configurations possible with each domain fraction, it does provide a qualitative basis for the onset of domain formation. In fact, the curve can be fitted quite well to the numerical data by means of a simple scaling factor, suggesting eqn (5) fundamentally captures the same underlying physics as the full model.

The above suggests that investigating the scaled model parameters that appear in eqn (5) can prove helpful in identifying ways to suppress the formation of domains. In Section 4, we already argued that the scaled square-gradient coefficient obeys the approximate relation $\kappa_f \approx l/L_0$, with l the mesh size of the network and L_0 the (initial) film thickness. Similarly, we point out that the energy of a mesogen with a permanent dipole moment, $\underline{p}$, subject to the electric field, $\underline{E}$, scales crucially with the mesogen orientation, such that we find $H \propto S_0|\underline{p}|^2|\underline{E}|^2$ for the orienting field, with S_0 the orientational order of the mesogens crosslinked into the polymer matrix (see also note 2).[31] The excluded-volume interactions opposing reorientation likewise depend strongly on the orientations of the mesogens, as well as their spatial dimensions, according to $H_* \propto S_0^2 a^2 r$, where we have assumed identical rod-like mesogens with length a and radius r.[31,55]

Subsequently recognising that the mesh size of the network, l, and the dipole moment of pendant mesogens, $|\underline{p}|$, must, all else being equal, also scale with the mesogen length, and inserting the result into eqn (5), we find

$$n = \frac{c_1 L_0}{a + c_2}\sqrt{\frac{1}{S_0 r} - c_3} + \frac{1}{2}, \tag{6}$$

with c_1, c_2, c_3 phenomenological fitting parameters. We thus conclude that the formation of domains can be suppressed by decreasing the initial thickness of the film, or by increasing either the linear dimensions of the mesogens, or the orientational order with which they are crosslinked into the network. We stress, however, that these modifications generally come at the cost of a decreased deformation magnitude,[31] meaning a trade-off is again unavoidable.

7 Conclusion and discussion

Inspired by the experiments of Van der Kooij and co-workers,[7] who report three distinct transient regimes, well-separated in the time domain, we investigate theoretically the transient dynamics of electrically-deforming liquid crystal network films. Although they argue these regimes originate from the sequential response of dipolar and cross-linked mesogens, followed by a progressive weakening of the polymer matrix, no concrete modelling or evidence is provided to lend support to this hypothesis. Making use of a non-local dynamical Landau theory that allows for viscoelastic relaxation, we propose an alternative explanation of their results in terms of permeation of the response of the local degree of order of a more mobile mesogen fraction followed by a volume expansion. Initially, this response must overcome the impact of thermal noise, subsequently reach saturation at the top of the film and finally permeate into the bulk.

We find the three time scales to only differ by at most an order of magnitude for the driving frequency used in this paper, implying that they are less well separated in time than the experimental ones.[7] Given the relatively simple nature of our Landau-type theory, where a host of complex mechanisms are effectively abstracted into a two-order-parameter theory and the response of the dynamics of the network itself enters only in a bulk modulus and local visco-elastic time scale, we should perhaps not be surprised.[31] Obviously, more research is required to settle this point.

In spite of this, our theory does make testable predictions. Indeed, the time scales characterising the transient dynamics depend strongly on the initial thickness of the film, giving rise to a thin-film-to-bulk transition that may distinguish our interpretation from the one proposed by Van der Kooij and co-workers. Likewise, the initial thickness of the film has a large effect on the magnitude of steady-state expansion, which increases with film thickness. On the other hand, this does come at the expense of establishing the steady-state oscillation more slowly. Notably, the magnitude of the expansion exhibits significant uncertainty beyond the thin-film-to-bulk transition.

This thin-film-to-bulk transition coincides with the onset of the formation of random domains in our one-dimensional model, which rationalises both the slower establishment of a steady-state oscillation, and variable actuation beyond the transition. We hypothesise that in three spatial dimensions, such random domains may well give rise to uncontrolled lateral patterning for which there is indeed experimental evidence.[6] Using simple linear-stability arguments, we infer that domain formation can be suppressed by decreasing the initial thickness of the film, increasing the linear dimensions of the mesogens, or the orientational order with which they are cross-linked into the network.

It is clear that our model provides only a crude description of liquid crystalline networks, yet it does provide a concrete basis for arguments as well as testable predictions. As such, our work contributes to the realisation of finer control over and greater understanding of the time scales on which liquid crystal network materials can be activated.

Author contributions

Guido L. A. Kusters: conceptualisation, formal analysis, investigation, methodology, software, validation, visualisation, writing – original draft. Paul van der Schoot: conceptualisation, funding acquisition, resources, supervision, writing – review and editing. Cornelis Storm: conceptualisation, funding acquisition, resources, supervision, writing – review and editing.

Conflicts of interest

There are no conflicts to declare.

Acknowledgements

This research received funding from the Dutch Research Council (NWO) in the context of the Soft Advanced Materials (SAM) consortium in the framework of the ENW PPP Fund for the top sectors and from the Ministry of Economic Affairs in the framework of the 'PPS-Toeslagregeling'.

References

1 H. Finkelmann, H.-J. Kock and G. Rehage, *Makromol. Chem., Rapid Commun.*, 1981, **2**, 317–322.
2 A. Cao, R. J. van Raak, X. Pan and D. J. Broer, *Adv. Funct. Mater.*, 2019, **29**, 1900857.
3 G. Babakhanova, A. P. Schenning, D. J. Broer and O. D. Lavrentovich, *Emerging Liquid Crystal Technologies XIV*, 2019, p. 109410I.
4 T. J. White, *J. Polym. Sci. Pol. Phys.*, 2012, **50**, 877–880.
5 J. E. Stumpel, D. J. Broer and A. P. Schenning, *Chem. Commun.*, 2014, **50**, 15839–15848.
6 D. Liu, N. B. Tito and D. J. Broer, *Nat. Commun.*, 2017, **8**, 1526.
7 H. M. van der Kooij, S. A. Semerdzhiev, J. Buijs, D. J. Broer, D. Liu and J. Sprakel, *Nat. Commun.*, 2019, **10**, 1–9.
8 H. M. van der Kooij, D. J. Broer, D. Liu and J. Sprakel, *ACS Appl. Mater. Interfaces*, 2020, **12**, 19927–19937.
9 H. Wermter and H. Finkelmann, *e-Polymers*, 2001, **1**, 13.
10 T. Ikeda, J. Mamiya and Y. Yu, *Angew. Chem., Int. Ed.*, 2007, **46**, 506–528.
11 A. Sánchez-Ferrer, T. Fischl, M. Stubenrauch, H. Wurmus, M. Hoffmann and H. Finkelmann, *Macromol. Chem. Phys.*, 2009, **210**, 1671–1677.
12 A. Sánchez-Ferrer, T. Fischl, M. Stubenrauch, A. Albrecht, H. Wurmus, M. Hoffmann and H. Finkelmann, *Adv. Mater.*, 2011, **23**, 4526–4530.
13 M. Dai, O. T. Picot, J. M. Verjans, L. T. de Haan, A. P. Schenning, T. Peijs and C. W. Bastiaansen, *ACS Appl. Mater. Interfaces*, 2013, **5**, 4945–4950.
14 S. Schuhladen, F. Preller, R. Rix, S. Petsch, R. Zentel and H. Zappe, *Adv. Mater.*, 2014, **26**, 7247–7251.
15 H. Zeng, O. M. Wani, P. Wasylczyk, R. Kaczmarek and A. Priimagi, *Adv. Mater.*, 2017, **29**, 1701814.
16 I. A. Rousseau and P. T. Mather, *J. Am. Chem. Soc.*, 2003, **125**, 15300–15301.
17 C. Liu, H. Qin and P. Mather, *J. Mater. Chem.*, 2007, **17**, 1543–1558.
18 K. A. Burke and P. T. Mather, *J. Mater. Chem.*, 2010, **20**, 3449–3457.
19 K. A. Burke and P. T. Mather, *Polymer*, 2013, **54**, 2808–2820.
20 A. Kotikian, R. L. Truby, J. W. Boley, T. J. White and J. A. Lewis, *Adv. Mater.*, 2018, **30**, 1706164.
21 E. Campo, J. Roig, B. Roeder, D. Wenn, B. Mamojka, M. Omastova, E. Terentjev and J. Esteve, *Nano-Opto-Mechanical Systems (NOMS)*, 2011, p. 81070H.
22 C. J. Camargo, N. Torras, H. Campanella, J. E. Marshall, K. Zinoviev, E. M. Campo, E. M. Terentjev and J. Esteve, *Nano-Opto-Mechanical Systems (NOMS)*, 2011, p. 810709.
23 C. J. Camargo, H. Campanella, J. E. Marshall, N. Torras, K. Zinoviev, E. M. Terentjev and J. Esteve, *Macromol. Rapid Comm.*, 2011, **32**, 1953–1959.
24 C. Camargo, H. Campanella, J. Marshall, N. Torras, K. Zinoviev, E. Terentjev and J. Esteve, *J. Micromech. Microeng.*, 2012, **22**, 075009.
25 N. Torras, K. Zinoviev, C. Camargo, E. M. Campo, H. Campanella, J. Esteve, J. Marshall, E. Terentjev, M. Omastová and I. Krupa, *et al.*, *Sens. Actuators, A*, 2014, **208**, 104–112.
26 D. Liu, C. W. Bastiaansen, J. M. den Toonder and D. J. Broer, *Angew. Chem., Int. Ed.*, 2012, **51**, 892–896.
27 M. E. McConney, A. Martinez, V. P. Tondiglia, K. M. Lee, D. Langley, I. I. Smalyukh and T. J. White, *Adv. Mater.*, 2013, **25**, 5880–5885.
28 D. Liu and D. J. Broer, *Angew. Chem., Int. Ed.*, 2014, **53**, 4542–4546.
29 A. H. Gelebart, D. Liu, D. J. Mulder, K. H. J. Leunissen, J. van Gerven, A. P. H. J. Schenning and D. J. Broer, *Adv. Funct. Mater.*, 2018, **28**, 1705942.

30 Y. Zhan, W. Zhang, A. Özden, S. Houben, M. Schuster, H. Gojzewski, G. Zhou, D. J. Broer and D. Liu, *ACS Appl. Polym. Mater.*, 2020, **2**, 4071–4077.
31 G. L. A. Kusters, I. P. Verheul, N. B. Tito, P. van der Schoot and C. Storm, *Phys. Rev. E*, 2020, **102**, 042703.
32 G. L. A. Kusters, N. B. Tito, C. Storm and P. van der Schoot, *Phys. Rev. E*, 2021, **104**, 054701.
33 M. Warner, K. P. Gelling and T. A. Vilgis, *J. Chem. Phys.*, 1988, **88**, 4008–4013.
34 M. Warner and X. J. Wang, *Macromolecules*, 1991, **24**, 4932–4941.
35 P. Bladon, E. M. Terentjev and M. Warner, *Phys. Rev. E*, 1993, **47**, R3838.
36 G. C. Verwey, M. Warner and E. M. Terentjev, *J. Phys. II France*, 1996, **6**, 1273–1290.
37 A. R. Tajbakhsh and E. M. Terentjev, *Eur. Phys. J. E: Soft Matter Biol. Phys.*, 2001, **6**, 181–188.
38 L. Golubović and T. C. Lubensky, *Phys. Rev. Lett.*, 1989, **63**, 1082.
39 M. Warner, P. Bladon and E. M. Terentjev, *J. Phys. II France*, 1994, **4**, 93–102.
40 P. D. Olmsted, *J. Phys. II France*, 1994, **4**, 2215–2230.
41 G. C. Verwey and M. Warner, *Macromolecules*, 1995, **28**, 4303–4306.
42 P. Martinoty, P. Stein, H. Finkelmann, H. Pleiner and H. R. Brand, *Eur. Phys. J. E: Soft Matter Biol. Phys.*, 2004, **14**, 311–321.
43 E. M. Terentjev and M. Warner, *Eur. Phys. J. E: Soft Matter Biol. Phys.*, 2004, **14**, 323–327.
44 O. Stenull and T. C. Lubensky, *Eur. Phys. J. E: Soft Matter Biol. Phys.*, 2004, **14**, 333–337.
45 P. Martinoty, P. Stein, H. Finkelmann, H. Pleiner and H. R. Brand, *Eur. Phys. J. E: Soft Matter Biol. Phys.*, 2004, **14**, 329–332.
46 P. Martinoty, P. Stein, H. Finkelmann, H. Pleiner and H. R. Brand, *Eur. Phys. J. E: Soft Matter Biol. Phys.*, 2004, **14**, 339–340.
47 A. M. Menzel, H. Pleiner and H. R. Brand, *Eur. Phys. J. E: Soft Matter Biol. Phys.*, 2009, **30**, 371.
48 G. L. A. Kusters, MSc thesis, Eindhoven University of Technology, Eindhoven, The Netherlands, 2020.
49 R. J. Glauber, *J. Math. Phys.*, 1963, **4**, 294–307.
50 P. G. de Gennes and J. Prost, *The Physics of Liquid Crystals*, Clarendon Press, 1995.
51 W. H. de Jeu, *Liquid crystal elastomers: materials and applications*, Springer, 2012, vol. 250.
52 G. Vertogen and W. H. de Jeu, *Thermotropic liquid crystals, fundamentals*, Springer Science & Business Media, 2012, vol. 45.
53 H. Fujikake, T. Murashige, H. Sato, M. Kawakita and H. Kikuchi, *Jpn. J. Appl. Phys.*, 2003, **42**, L60.
54 A. Y.-G. Fuh, M.-S. T. M.-S. Tsai and C.-Y. H. C.-Y. Huang, *Jpn. J. Appl. Phys.*, 1996, **35**, 3960.
55 L. Onsager, *Ann. N. Y. Acad. Sci.*, 1949, **51**, 627–659.

